



**HAL**  
open science

# Multiple-stage Precursor Ion Separation and High Resolution Mass Spectrometry toward Structural Characterization of 2,3-Diacyltrehalose Family from *Mycobacterium tuberculosis*

Cheryl Frankfater, Robert Abramovitch, Georgiana Purdy, John Turk, Laurent Legentil, Loïc Lemiègre, Fong-Fu Hsu

## ► To cite this version:

Cheryl Frankfater, Robert Abramovitch, Georgiana Purdy, John Turk, Laurent Legentil, et al.. Multiple-stage Precursor Ion Separation and High Resolution Mass Spectrometry toward Structural Characterization of 2,3-Diacyltrehalose Family from *Mycobacterium tuberculosis*. *Separations*, 2019, 6 (1), pp.4. 10.3390/separations6010004 . hal-02115766

**HAL Id: hal-02115766**

**<https://univ-rennes.hal.science/hal-02115766>**

Submitted on 1 Apr 2020

**HAL** is a multi-disciplinary open access archive for the deposit and dissemination of scientific research documents, whether they are published or not. The documents may come from teaching and research institutions in France or abroad, or from public or private research centers.

L'archive ouverte pluridisciplinaire **HAL**, est destinée au dépôt et à la diffusion de documents scientifiques de niveau recherche, publiés ou non, émanant des établissements d'enseignement et de recherche français ou étrangers, des laboratoires publics ou privés.

Article

# Multiple-stage Precursor Ion Separation and High Resolution Mass Spectrometry toward Structural Characterization of 2,3-Diacyltrehalose Family from *Mycobacterium tuberculosis*

Cheryl Frankfater <sup>1,†</sup>, Robert B. Abramovitch <sup>2,†</sup> , Georgiana E. Purdy <sup>3,†</sup>, John Turk <sup>1</sup>, Laurent Legentil <sup>4</sup> , Loïc Lemiègre <sup>4</sup>  and Fong-Fu Hsu <sup>1,\*</sup> 

<sup>1</sup> Department of Medicine, Washington University School of Medicine, St. Louis, MO 63110, USA; c.frankf@wustl.edu (C.F.); jturk@wustl.edu (J.T.)

<sup>2</sup> Department of Microbiology and Molecular Genetics, Michigan State University, East Lansing, MI 48824, USA; abramov5@msu.edu

<sup>3</sup> Department of Molecular Microbiology and Immunology, Oregon Health & Science University, Portland, OR 97239, USA; purdyg@ohsu.edu

<sup>4</sup> Univ Rennes, Ecole Nationale Supérieure de Chimie de Rennes, CNRS, ISCR-UMR 6226, F-35000 Rennes, France; laurent.legentil@ensc-rennes.fr (L.L.); loic.lemiegre@ensc-rennes.fr (L.L.)

\* Correspondence: fhsu@im.wustl.edu; Tel.: +1-314-362-0056

† These authors contributed equally as co-first author.

Received: 1 December 2018; Accepted: 7 January 2019; Published: 15 January 2019



**Abstract:** Mass spectrometry (MS)-based precursor ion isolation, collision-induced dissociation (CID) fragmentation, and detection using linear ion-trap multiple-stage mass spectrometry (LIT MS<sup>n</sup>) in combination with high resolution mass spectrometry (HRMS) provides a unique tool for structural characterization of complex mixture without chromatographic separation. This approach permits not only separation of various lipid families and their subfamilies, but also stereoisomers, thereby, revealing the structural details. In this report, we describe the LIT MS<sup>n</sup> approach to unveil the structures of a 2,3-diacyl trehalose (DAT) family isolated from the cell envelope of *Mycobacterium tuberculosis*, in which more than 30 molecular species, and each species consisting of up to six isomeric structures were found. LIT MS<sup>n</sup> performed on both [M + Na]<sup>+</sup> and [M + HCO<sub>2</sub>]<sup>-</sup> ions of DAT yield complimentary structural information for near complete characterization of the molecules, including the location of the fatty acyl substituents on the trehalose backbone. This latter information is based on the findings of the differential losses of the two fatty acyl chains in the MS<sup>2</sup> and MS<sup>3</sup> spectra; while the product ion spectra from higher stage LIT MS<sup>n</sup> permit confirmation of the structural assignment.

**Keywords:** tandem mass spectrometry; linear ion trap; glycolipid; diacyltrehalose; *Mycobacterium tuberculosis*

## 1. Introduction

Tandem mass spectrometry is a powerful tool for structural analysis of unknown molecules. Tandem mass spectrometry consists of several sequential events including formation and mass selection of the precursor ions, collision induced dissociation (CID) with inert target gas for fragment ion formation, followed by mass analysis and detection of the product-ions. For tandem mass spectrometry with quadrupole (e.g., triple quadrupole, TSQ), sector, and hybrid Q-TOF instruments, these processes occur sequentially in the separate regions of the instruments and the MS/MS process is tandem-in-space. For quadrupole ion-trap (QIT) and linear ion trap (LIT) instruments, the precursor ion

selection, CID, and product-ion analysis and detection events are all executed in the ion trap in a timing sequence manner, and the MS/MS process is tandem-in-time [1]. Linear ion trap multiple stage tandem mass spectrometry (LIT MS<sup>n</sup>) permits the repeat of the precursor ion selection-CID-product-ion analysis process, and up to 10 cycles can be performed using modern commercial LIT mass spectrometers such as Thermo LTQ Orbitrap. This instrument is also featured with an extreme high resolving power and up to a million resolution (at m/z 200) can be reached [2].

Due to its MS<sup>n</sup> capability with high resolution, LIT/Orbitrap with MS<sup>n</sup> approach has been widely used in the structural characterization of a wide range of biomolecules [3–7]. LIT MS<sup>n</sup> with high resolution is also extremely useful for identification of complex lipid structures, in particular, microbial lipid, permitting revelation of numerous isomeric molecules in lipid extracts. For example, we demonstrated that sulfolipid II in *Mycobacterium tuberculosis* (*M. tuberculosis*) H37Rv cells is the predominated lipid family, consisting of hundreds of molecular species rather than the sulfolipid I family as previously reported [8,9]. LIT MS<sup>n</sup> with high resolution mass spectrometry has also been successfully applied to delineate the structures of phosphatidylinositol mannosides (PIMs) [10,11], and phthiocerol dimycocerosates (PDIMs) [12] in the cell envelope of *M. tuberculosis*. The former lipid family is known to have played important roles in *M. tuberculosis* adhesins that mediate attachment to nonphagocytic cells [13], while the latter is recently found to play role in drug resistance to *M. tuberculosis* [14].

In addition to the above complex lipid families, other glycolipids found in the mycobacterial cell wall include acylated trehaloses [15–18]. These trehalose-containing glycolipids consist of many families [18–22], of which the 2,3-di-O-acyltrehalose (DAT) family was previously defined as glycolipid B. DAT is a mycobacterial factor capable of modulating host immune responses [23] and can inhibit the proliferation of murine T cells [24]. DAT along with pentaacyl trehalose (PAT) also play an important role in pathogenesis and a structural role in the cell envelope, promoting the intracellular survival of the bacterium [25]. The DATs from *M. tuberculosis* and *M. fortuitum* have been shown to be antigenic [24,26,27] and their potential use in serodiagnosis has been postulated [28,29].

Besra and coworker defined the structures of the acylated trehalose lipid family using gas chromatography-mass spectrometry, in conjunction with normal/reversed phase TLC, and one/two-dimensional <sup>1</sup>H, and <sup>13</sup>C nuclear magnetic resonance spectroscopy [21]. However, there is no report in the detailed structural assignment of the various molecular species with many isomeric structures for the entire lipid family.

In this report, we applied multiple stage precursor ion isolation and resonance excitation activation to generate distinct MS<sup>n</sup> spectra to explore the structure details of the 2,3-diacyl trehalose (DAT) lipid family found in *M. tuberculosis*. This study highlights the unique feature of the technique of LIT MS<sup>n</sup> for tandem-in-time precursor ion separation that affords structural characterization of a complex lipid family, while a similar structural analysis would be very difficult to perform utilizing the tandem mass spectrometric approach with a sector, TSQ or QTOF instrument.

## 2. Materials and Methods

### 2.1. Materials

All solvents (spectroscopic grade) and chemicals (ACS grade) were obtained from Sigma Chemical Co. (St. Louis, MO, USA).

### 2.2. Sample Preparation

*M. tuberculosis* strain H37Rv were grown and total lipids were extracted and isolated as previously described [8]. Briefly, the total lipid was separated by a Phenomenex C18 Kinetex (100 × 4.6 mm, pore size 100 Å, particle size 2.6 μm) column at a flow rate of 300 μL/min with a gradient system as previously described [12]. DAT (eluted at 24.45–26.43 min) fraction from three injections (~200 μg total

lipid/injection) were collected and pooled, dried under a stream of nitrogen, and stored at  $-20\text{ }^{\circ}\text{C}$  until use.

### 2.3. Mass Spectrometry

Both high-resolution ( $R = 100,000$  at  $m/z$  400) low-energy CID and higher collision-energy dissociation (HCD) tandem mass spectrometric experiments were conducted on a Thermo Scientific (San Jose, CA, USA) LTQ Orbitrap Velos mass spectrometer (MS) with Xcalibur operating system. Samples in  $\text{CH}_3\text{OH}$  were infused ( $1.5\ \mu\text{L}/\text{min}$ ;  $\sim 10\ \text{pmol}/\mu\text{L}$ ) to the ESI source, where the skimmer was set at ground potential, the electrospray needle was set at  $4.0\ \text{kV}$ , and temperature of the heated capillary was  $300\text{ }^{\circ}\text{C}$ . The automatic gain control of the ion trap was set to  $5 \times 10^4$ , with a maximum injection time of  $100\ \text{ms}$ . Helium was used as the buffer and collision gas at a pressure of  $1 \times 10^{-3}\ \text{mbar}$  ( $0.75\ \text{mTorr}$ ). The  $\text{MS}^n$  experiments were carried out with an optimized relative collision energy ranging from  $25\text{--}35\%$  and with an activation  $q$  value at  $0.25$ . The activation time was set for  $10\ \text{ms}$  to leave a minimal residual abundance of precursor ion (around  $20\%$ ). For the HCD experiments, the collision energy was set at  $50\text{--}55\%$  and mass scanned from  $m/z$  100 to the upper  $m/z$  value that covers the precursor ions. The mass selection window for the precursor ions was set at  $1\ \text{Da}$  wide to admit the monoisotopic peak to the ion-trap for collision-induced dissociation (CID) for unit resolution detection in the ion-trap or high resolution accurate mass detection in the Orbitrap mass analyzer. Mass spectra were accumulated in the profile mode, typically for  $3\text{--}10\ \text{min}$  for  $\text{MS}^n$  spectra ( $n = 2,3,4$ ).

### 2.4. Nomenclature

To facilitate data interpretation, the following abbreviations were adopted. The abbreviation of the long-chain fatty acid such as the stearic acid attached to the C2 position of the trehalose backbone is designated as 18:0. The multiple methyl-branched mycolipenic acid, for example, the 2,4,6-trimethyl-2-tetracosenoic acid attached to the C3-position is designated as 27:1 to reflect the fact that the acid contains a  $\text{C}_{27}$  acyl chain with one double bond. Therefore, the DAT species consisting of 18:0- and 27:1-FA substituents at C2-, and C3-position, respectively, is designated as 18:0/27:1-DAT.

## 3. Results and Discussion

DAT formed  $[\text{M} + \text{Alk}]^+$  ions ( $\text{Alk} = \text{NH}_4, \text{Li}, \text{Na}, \text{etc.}$ ) in the positive ion mode; and  $[\text{M} + \text{X}]^-$  ( $\text{X} = \text{Cl}, \text{RCO}_2; \text{R} = \text{H}, \text{CH}_3, \text{C}_2\text{H}_5, \text{etc.}$ ) ions in the negative-ion mode when subjected to ESI in the presence of  $\text{Alk}^+$  and  $\text{X}^-$ . For example, when dissolved in  $\text{CH}_3\text{OH}$  with the presence of  $\text{HCO}_2\text{Na}$ , adduct ions in the fashions of  $[\text{M} + \text{Na}]^+$  (Figure 1) in the positive ion mode and  $[\text{M} + \text{HCO}_2]^-$  ions (data not shown) in the negative ion mode were observed. The formation of these adduct ions was revealed by the elemental composition of the molecular species deduced by high resolution mass spectrometry (Table 1). Upon being subject to CID in a linear ion-trap, the  $\text{MS}^n$  ( $n = 2,3,4$ ) spectra of both the  $[\text{M} + \text{Na}]^+$  and  $[\text{M} + \text{HCO}_2]^-$  ions contain rich structural information readily applicable for structural identification.

**Table 1.** The high resolution mass measurements of the [M + Na]<sup>+</sup> ions of DATs isolated from *M. tuberculosis* and the assigned structures (\* structure not defined).

Measured m/z	Theo. Mass m/z	Deviation mmu	Rel. Intensity %	Ele. Composition	Major structures	Minor structures
935.6436	935.6430	0.55	3.42	C51H92O13Na	14:1/25:1	12:1/27:1
937.6594	937.6587	0.73	4.34	C51H94O13Na	14:0/25:1	12:0/27:1; 16:1/23:0; 15:1/24:0; 13:0/26:1
939.6747	939.6743	0.37	1.48	C51H96O13Na	*	
949.6585	949.6587	−0.19	6.58	C52H94O13Na	16:1/24:1	
951.6742	951.6743	−0.15	20.8	C52H96O13Na	16:1/24:0	16:0/24:1; 15:0/25:1; 17:1/23:0; 14:0/26:1; 13:0/27:1
953.6898	953.6900	−0.12	18.49	C52H98O13Na	16:0/24:0	
961.6587	961.6587	0.01	4.31	C53H94O13Na	*	
963.6743	963.6743	−0.05	44.16	C53H96O13Na	16:1/25:1; 14:1/27:1	
965.6898	965.6900	−0.12	50.07	C53H98O13Na	16:0/25:1	14:0/27:1; 18:0/23:1
967.7054	967.7056	−0.22	12.26	C53H100O13Na	18:0/23:0; 17:0/24:0	16:0/25:0
975.6740	975.6743	−0.3	3.03	C54H96O13Na	*	
977.6899	977.6900	−0.06	25.16	C54H98O13Na	16:1/26:1	
979.7056	979.7056	−0.06	54.48	C54H100O13Na	18:0/24:1; 18:1/24:0	16:0/26:1; 17:0/25:1; 16:1/26:0; 15:0/27:1
981.7211	981.7213	−0.15	62.62	C54H102O13Na	18:0/24:0	17:0/25:0; 16:0/26:0
989.6898	989.6900	−0.17	18.03	C55H98O13Na	16:1/27:2	
991.7054	991.7056	−0.2	100	C55H100O13Na	16:1/27:1	18:1/25:1; 16:0/27:2; 17:0/26:2
993.7210	993.7213	−0.29	95.91	C55H102O13Na	16:0/27:1	18:0/25:1; 17:0/26:1
1005.7211	1005.7213	−0.2	34.31	C56H102O13Na	16:1/28:1; 17:1/27:1	17:0/27:2; 18:1/26:1; 18:0/26:2
1007.7366	1007.7369	−0.31	51.54	C56H104O13Na	17:0/27:1	16:0/28:1; 18:0/26:1; 19:0/25:1; 16:1/28:0 20:0/24:0
1009.7518	1009.7526	−0.75	7.65	C56H106O13Na	18:0/26:0	
1017.7209	1017.7213	−0.38	11.79	C57H102O13Na	18:1/27:2	
1019.7367	1019.7369	−0.25	52.39	C57H104O13Na	18:1/27:1	18:0/27:2; 17:1/28:1
1021.7522	1021.7526	−0.37	92.1	C57H106O13Na	18:0/27:1	17:0/28:1
1033.7521	1033.7526	−0.47	10.49	C58H106O13Na	18:1/28:1	19:0/27:2; 19:1/27:1; 18:0/28:2; 19:0/27:2
1035.7678	1035.7682	−0.45	13.33	C58H108O13Na	19:0/27:1; 18:0/28:1	18:1/28:0; 17:0/29:1
1047.7677	1047.7682	−0.5	2.56	C59H108O13Na	18:0/28:2	
1049.7835	1049.7839	−0.31	5.47	C59H110O13Na	19:0/28:1	20:0/27:1; 18:0/29:1; 17:0/30:1
1061.7837	1061.7839	−0.19	1.63	C60H110O13Na	18:1/30:1	
1063.7991	1063.7995	−0.38	1.83	C60H112O13Na	18:0/30:1	

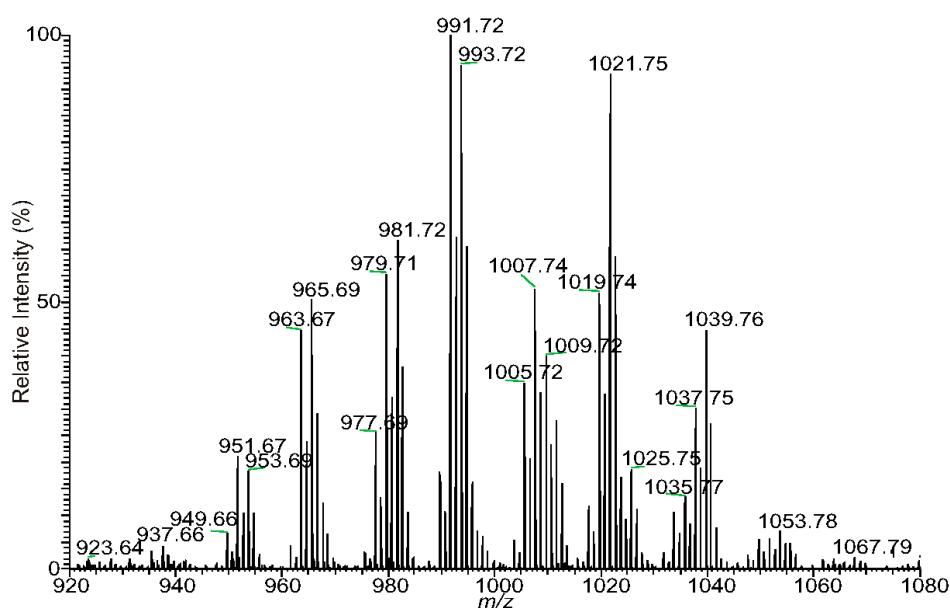


**Figure 1.** The positive-ion ESI mass spectrum of the  $[M + Na]^+$  ions of the DAT species isolated from cell envelope of *M. tuberculosis*.

### 3.1. The Fragmentation Processes of the $[M + Na]^+$ Ions of DAT Revealed by LIT MS<sup>n</sup>

The utility in the performance of sequential precursor ion separation, CID, and acquiring MS<sup>n</sup> spectra of LIT MS<sup>n</sup> mass spectrometry permits insight into not only the fragmentation processes, but also the structural details of the molecules. For example, the LIT MS<sup>2</sup> spectrum of the  $[M + Na]^+$  ions of 18:0/27:1-DAT at  $m/z$  1021 contained the dominated ions of  $m/z$  859 (Figure 2a) arising from loss of glucose residue, along with the ion set at  $m/z$  737 and 613, arising from losses of 18:0-, and 27:1-fatty acid substituents, respectively (Scheme 1). The ions of  $m/z$  859 represent the sodiated diacylglycerol with both the 18:0-, and 27:1-fatty acyl substituents. This notion is further supported by the MS<sup>3</sup> spectrum of the ions of  $m/z$  859 ( $1021 \rightarrow 859$ , Figure 2b) which contained ions of  $m/z$  575 ( $859 - 284$ ) and 451 ( $859 - 408$ ), arising from losses of 18:0-, and 27:1-fatty acid substituents, respectively. The results also suggest that the Na<sup>+</sup> charge site most likely resides at the glucose ring with the two acyl groups (Glc 1). In contrast, the MS<sup>2</sup> spectrum of the  $[M + Na]^+$  ions of the 6,6'-dioleoyltrehalose standard [30] at  $m/z$  893 forms abundant ions at  $m/z$  467, representing the sodiated oleoylglycerol (data not shown), consistent with the fact that the 18:1 fatty acyl substituents in the 18:1/18:1-DAT are located on the separate Glc (i.e., Glc1 and Glc 2). Further dissociation of the ions of  $m/z$  737 ( $1013 \rightarrow 737$ , Figure 2c) gave rise to the prominent ions of  $m/z$  329 by loss of 27:1-fatty acid substituent, and  $m/z$  575, arising from loss of glucose residue (Glc 2), together with  $m/z$  431 representing a sodiated ion of 27:1-FA. These results further support the fragmentation processes as proposed in Scheme 1.

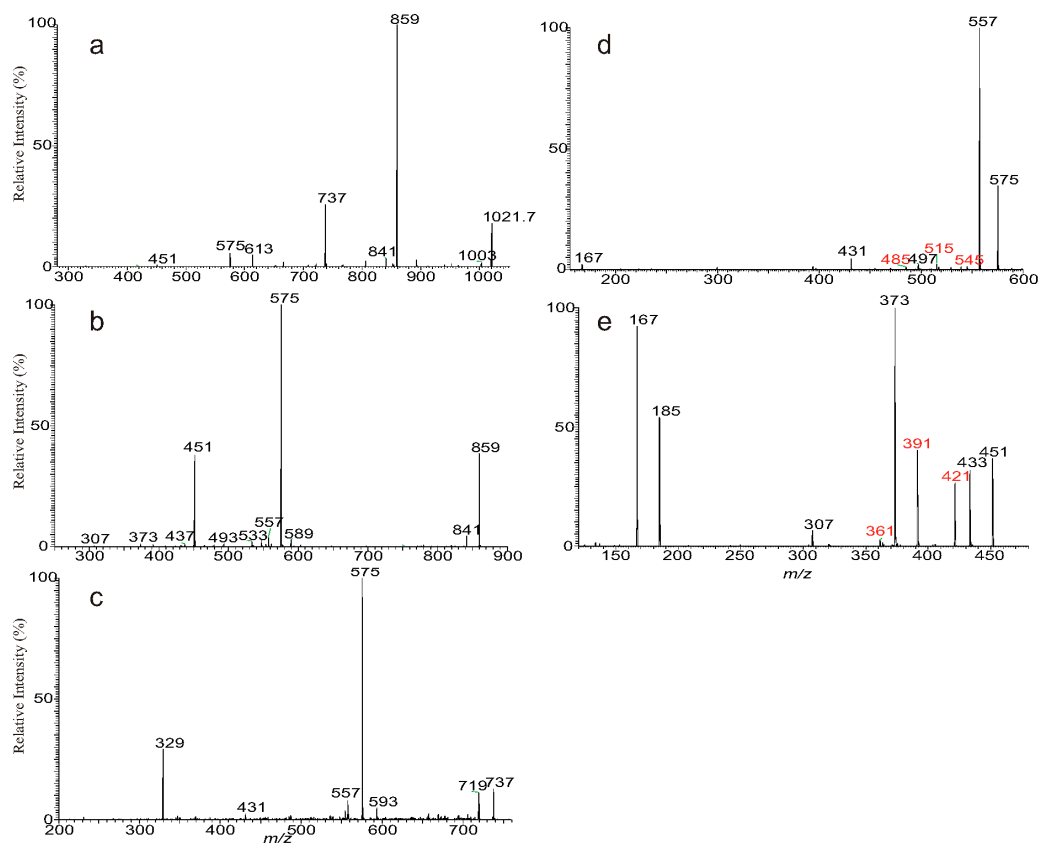
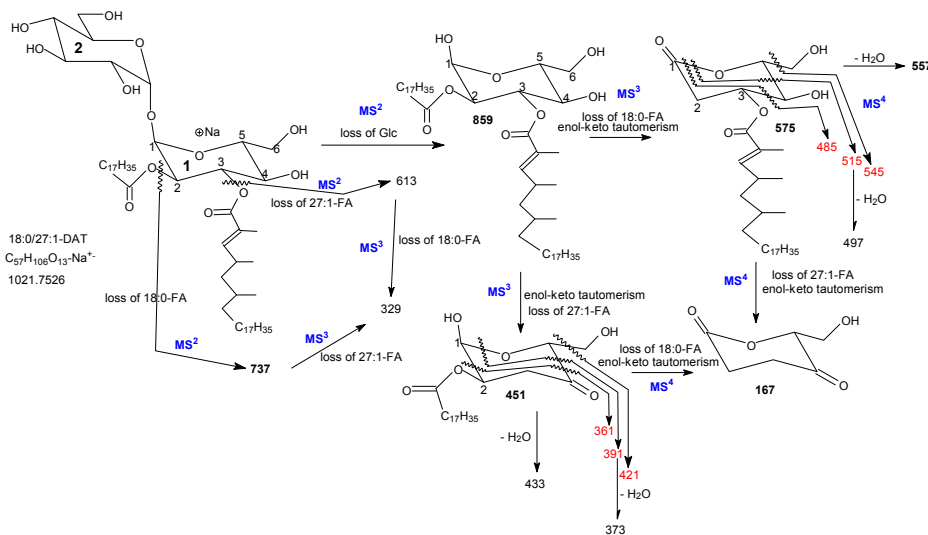


**Figure 2.** The LIT MS<sup>2</sup> spectrum of the [M + Na]<sup>+</sup> ion of 18:0/27:1-DAT at m/z 1021 (a), its MS<sup>3</sup> spectra of the ions of m/z 859 (1021 → 859) (b), and of m/z 737 (1021 → 737) (c); and its MS<sup>4</sup> spectra of the ions of m/z 575 (1021 → 859 → 575) (d), and of m/z 451 (1021 → 859 → 451) (e).



**Scheme 1.** The structure of [M + Na]<sup>+</sup> ion of 18:0/27:1-DAT at m/z 1021 and proposed LIT MS<sup>n</sup> fragmentation processes\*. \* All the ions represent the sodiated species. To simplify, the drawing of “Na<sup>+</sup>” is omitted from the scheme.

The formation of the ions of m/z 575 from m/z 859 by loss of 18:0-FA residue at C2 may involve the participation of the hydrogen atom at C1 to form an enol, which undergoes enol-keto tautomerism to yield a stable sodiated ion of monoacyl (27:1) glucose as the keto form (Scheme 1). This fragmentation processes are further supported by MS<sup>4</sup> on the ions of m/z 575 (1013 → 859 → 575, Figure 2d), which

yielded ions of  $m/z$  545, 515, and 475, likely arising from the across cleavages of the glucose ring, suggesting that the 27:1-fatty acyl substituent is located at C3 (Scheme 1).

Similarly,  $MS^4$  on the ion of  $m/z$  451 ( $1013 \rightarrow 859 \rightarrow 451$ , Figure 2e) gave rise to ions of  $m/z$  421, 391, and 361 arising from the similar rupture of the glucose ring, indicating that the 18:0-fatty acyl substituent is most likely located at C2 of the glucose ring. The preliminary loss of the 27:1-FA substituent may involve the participation of the adjacent hydrogen at C4 of Glc 1 to form an enol, which sequentially rearranges to keto form via the similar enol-keto tautomerism mechanism.

The preferential formation of the ions of  $m/z$  575 from loss of the 18:0-FA substituent over the ions of  $m/z$  451 from similar loss of the 27:1-FA as seen in Figure 2a is readily applicable for locating the FA substituents on the trehalose backbone.

### 3.2. LIT $MS^n$ on the $[M + Na]^+$ Ions of DAT for Stereoisomer Recognition

To define the structures of DAT species with many isomeric structures using LIT  $MS^n$  is exemplified by characterization of the  $[M + Na]^+$  ions of  $m/z$  979, which gave rise to the prominent ions at  $m/z$  817 (Figure 3a) arising from loss of glucose. Further dissociation of the ions of  $m/z$  817 ( $979 \rightarrow 817$ ; Figure 3b) yielded the ion pairs of  $m/z$  533/451, arising from losses of 18:0/24:1 fatty acid substituents, indicating that these two acyl groups are situated at Glc 1, giving assignment of the 18:0/24:1-DAT structure. The spectrum also contained the  $m/z$  535/449, 561/423, 547/437, 563/421, 575/409 ion pairs, arising from losses of 18:1/24:0, 16:0/26:1, 17:0/25:1, 16:1/26:0, and 15:0/27:1 FA pairs, respectively. The results indicate the presence of the 18:1/24:0-, 16:0/26:1-, 17:0/25:1-, 16:1/26:0-, and 15:0/27:1-DAT isomers. The above structure assignments were further confirmed by the  $MS^3$  and  $MS^4$  spectra. For example, the  $MS^3$  spectrum of the ions of  $m/z$  697 ( $979 \rightarrow 697$ ; Figure 3c) from primary loss of a 18:1-FA residue at C2 (Figure 3a) gave the abundant ions of  $m/z$  535 (loss of Glc 2), along with ions of  $m/z$  329 arising from loss of 24:0-FA substituent, and of  $m/z$  391, representing a sodiated 24:0-FA cation. The results confirm the presence of 18:1/24:0-DAT. The  $MS^4$  spectrum of the ions of  $m/z$  535 ( $979 \rightarrow 817 \rightarrow 535$ ; Figure 3d) contained ions of  $m/z$  517 (loss of  $H_2O$ ) and 505, 475, 445 arising from cleavages of the sugar ring similar to that shown in Scheme 1, along with ions of  $m/z$  167 from loss of 24:0-FA, pointing to the notion that the 24:0-FA is located at C3.

The  $MS^3$  spectrum of the ions of  $m/z$  695 ( $979 \rightarrow 695$ ; Figure 3e) contained the ions of  $m/z$  533 and 329 arising from further losses of Glc and 24:1-FA residues (Figure 3a), respectively. The  $MS^4$  spectrum of the ions of  $m/z$  533 ( $979 \rightarrow 817 \rightarrow 533$ ; data not shown) gave ions of  $m/z$  503, 473, and 443 from the similar fragmentation processes that cleave the sugar ring (Scheme 1), confirming that the 24:1-FA substituent is located at C3. The results led to assign the 18:0/24:1-DAT structure. Using this LIT  $MS^n$  approach, a total of six isomeric structures were identified.

### 3.3. The Fragmentation Processes of the $[M + HCO_2]^-$ Ions of DAT Revealed by LIT $MS^n$

In the negative-ion mode in the presence of  $HCO_2^-$ , 18:0/27:1-DAT formed  $[M + HCO_2]^-$  ions of  $m/z$  1043, which gave rise to the prominent ions of  $m/z$  997 by loss of  $HCO_2H$ , along with ions of  $m/z$  713 and 589 by further losses of 18:0- and 27:1-FA substituents, respectively (Figure 4a) (Scheme 2). This fragmentation process is further supported by the  $MS^3$  spectrum of the ions of  $m/z$  997 ( $1043 \rightarrow 997$ , Figure 4b), which are equivalent to the  $[M - H]^-$  ions of 18:0/27:1-DAT. The ions of  $m/z$  731 (Figure 4a) arising from loss of 18:0-FA as a ketene is more prominent than the ions of  $m/z$  607 arising from analogous 27:1-ketene loss. This preferential formation of  $m/z$  731 corresponding to loss of the FA-ketene at C2 over ions of  $m/z$  607 from the FA-ketene loss at C3 was seen in all the  $MS^2$  spectra of the  $[M + HCO_2]^-$  ions of DAT, providing useful information for distinction of the FA substituents at C2 and C3. The ketene loss process probably involves the participation of  $HCO_2^-$ , which attracts the labile  $\alpha$ -hydrogen on the fatty acid group to eliminate FA-ketene and  $HCO_2H$  simultaneously (Scheme 2). Therefore, the low abundance of the ions of  $m/z$  607 arising from loss of the FA-ketene at C3 may reflect the fact that the 27:1-FA substituent at C3 contains an  $\alpha$ -methyl side chain [19,21,22,31],



and does not contain labile  $\alpha$ -hydrogen required for ketene loss. This is in contrast to the 18:0-FA substituent at C2, which possesses two  $\alpha$ -hydrogens (Scheme 2).

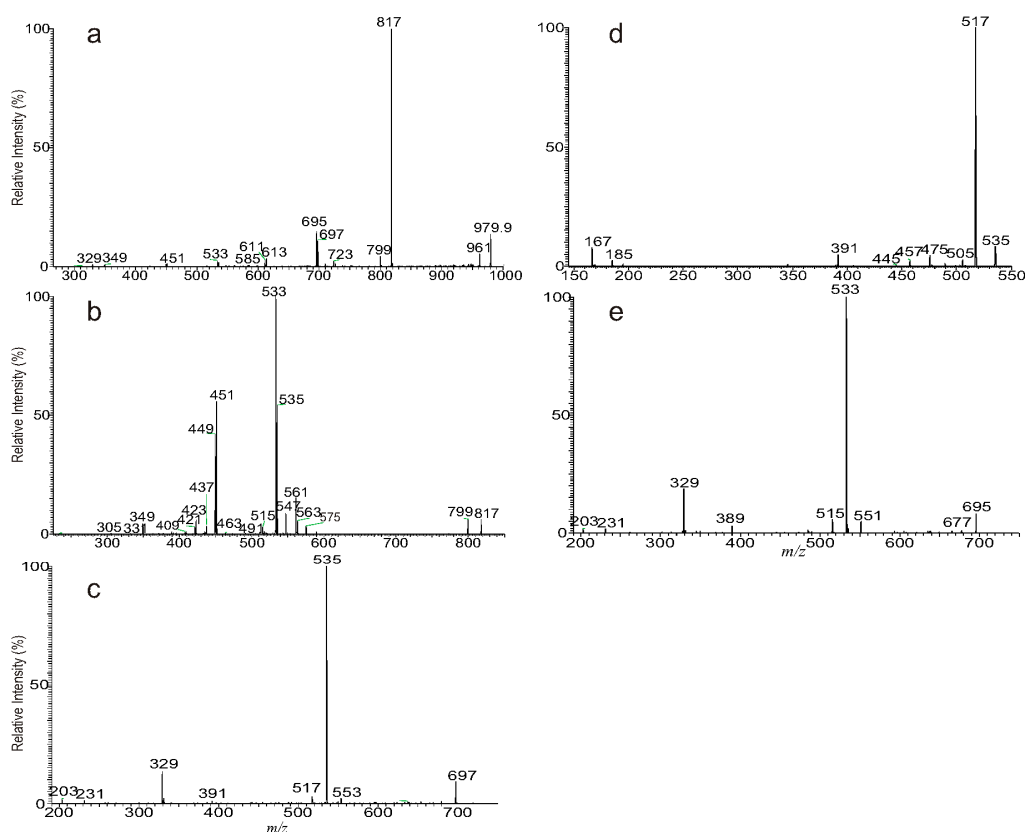


**Figure 3.** The MS<sup>2</sup> spectrum of the  $[M + Na]^+$  ions of m/z 979 (a), its MS<sup>3</sup> spectra of the ions of m/z 817 (979  $\rightarrow$  817) (b), of m/z 697 (979  $\rightarrow$  697) (c), its MS<sup>4</sup> spectrum of the ions of m/z 535 (979  $\rightarrow$  817  $\rightarrow$  535) (d); and the MS<sup>3</sup> spectrum of the ions of m/z 695 (979  $\rightarrow$  695) (e).

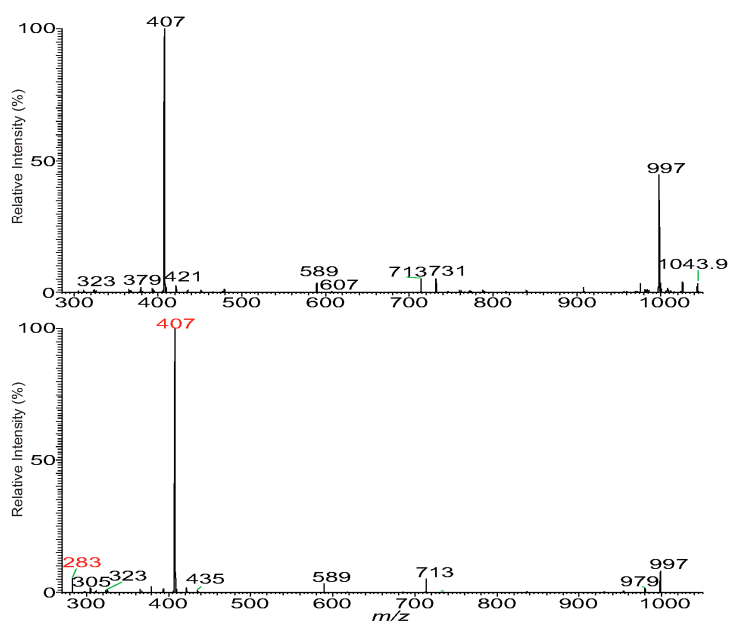
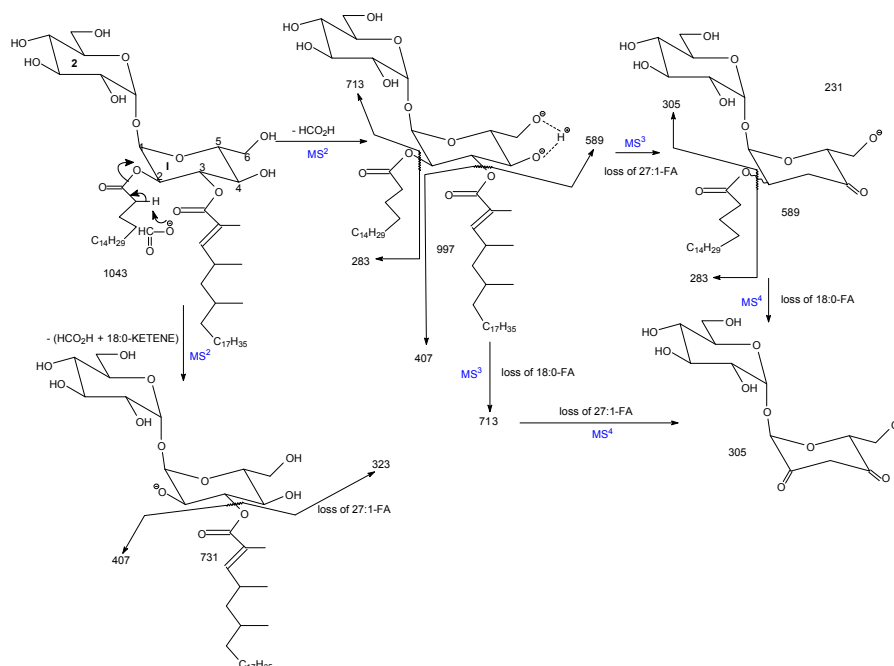


**Figure 4.** The negative-ion MS<sup>2</sup> spectrum of the  $[M + HCO_2]^-$  ions of 18:0/27:1-DAT at m/z 1043 (a), its MS<sup>3</sup> spectrum of the ions of m/z 997 (1043  $\rightarrow$  997) (b).



**Scheme 2.** The proposed LIT  $MS^n$  fragmentation processes of the  $[M + HCO_2]^-$  ions of 18:0/27:1-DAT at  $m/z$  1043.

The ions at  $m/z$  731 and 607 arising from losses of 18:0-ketene and 27:1-ketene, respectively, are absent in Figure 4b. This is consistent with the notion that the ketene loss requires the participation of  $HCO_2^-$ . The ketene loss pathway becomes not operative after the  $[M - H]^-$  ions are formed from  $[M + HCO_2]^-$  by loss of  $HCO_2H$ .

The spectrum (Figure 4b) also contained the prominent ions of  $m/z$  407, representing 27:1-fatty acid carboxylic anions, and the ions of  $m/z$  283 representing 18:0-FA carboxylate anions, along with ions of  $m/z$  305 arising from losses of both 18:0- and 27:1-FA substituents. The preferential formation of the ions of  $m/z$  407 (at C3) over  $m/z$  283 (at C2) is also a reflection of the location of the fatty acid substituents on the Glc ring, leading to the assignment of 18:0/27:1-DAT structure.

### 3.4. Recognition of Stereoisomers Applying LIT $MS^n$ on the $[M + HCO_2]^-$ Ions

Similarly, the  $MS^2$  spectrum of the ions of  $m/z$  1001 is dominated by the ions of  $m/z$  955 from loss of  $HCO_2H$  (Figure 5a). The  $MS^3$  spectrum of the ions of  $m/z$  955 ( $1001 \rightarrow 955$ ) (Figure 5b) contained ions at  $m/z$  701, 699, 685, 673, 671, 589, 587, 575, 561, 559, similar to those seen in Figure 5a, consistent with the consecutive dissociation processes of the  $[M - H]^-$  ions that eliminate the FA substituents. These ions arose from losses of 16:1-, 16:0-, 17:0-, 18:1-, 18:0-, 24:1-, 24:0-, 25:0-, 26:1-, and 26:0-fatty acid substituents, respectively. The spectrum also contained the major  $m/z$  283/365, 281/367 ion pairs, together with the minor ion pairs of  $m/z$  255/393, 253/395, 269/379, 241/407. These structural information led to assignment of the major 18:0/24:1-, and 18:1/24:0-DAT isomers, together with the 16:0/26:1-, 16:1/26:0-, 17:0/25:1, and 15:0/27:1-DAT minor isomers. It should be noted that the absence of ions at  $m/z$  241, 253, 255, and 269 representing 15:0-, 16:1-, 16:0-, and 17:0-carboxylate anions, respectively, in Figure 5b, are attributable to the low mass cutoff nature of an ion-trap instrument. In contrast, these ions are abundant in the HCD production ion spectrum (data not shown), similar to that obtained by a triple quadrupole instrument [32]. The location of the fatty acid substituent position on the glucose skeleton is again confirmed by observation of the ions corresponding to loss of the fatty acid substituents as ketenes. For example, ions at  $m/z$  691 and 689 (Figure 5a) derived from losses of  $(HCO_2H + 18:1\text{-ketene})$  and  $(HCO_2H + 18:0\text{-ketene})$ , respectively, pointing to the notion that both 18:1- and 18:0-FA are situated at C2 of the 18:1/24:0-, and 18:0/24:1-DAT isomers, respectively. The assigned

structure of 18:0/24:1-DAT, for example, is further confirmed by MS<sup>4</sup> on the ions of *m/z* 671 (1001 → 955 → 671) (Figure 5c), which formed ions of *m/z* 365, representing a 24:1-carboxylate anion, and ions of *m/z* 323 and 305 arising from further loss of 24:1-FA substituent as ketene and FA, respectively.

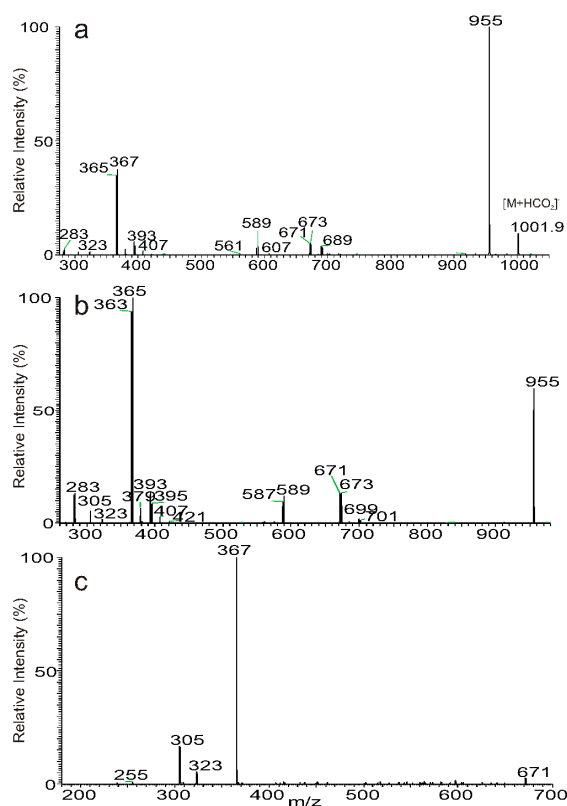


**Figure 5.** The negative-ion MS<sup>2</sup> spectrum of the [M + HCO<sub>2</sub>]<sup>-</sup> ions of *m/z* 1001 (a), its MS<sup>3</sup> spectrum of the ions of *m/z* 955 (1001 → 955) (b), and the MS<sup>4</sup> spectrum of the ions of *m/z* 671 (1001 → 955 → 671) (c).

### 3.5. Characterization of Minor Species Applying LIT MS<sup>n</sup> on the [M + HCO<sub>2</sub>]<sup>-</sup> Ions

Applying multiple-stage mass spectrometry (LIT MS<sup>n</sup>) for consecutive ion separation followed by CID mass spectrometry is particularly useful for characterization of minor DAT species as [M + HCO<sub>2</sub>]<sup>-</sup> ions. For example, the MS<sup>2</sup> spectrum of the [M + HCO<sub>2</sub>]<sup>-</sup> ion of the minor DAT at *m/z* 989 (Figure 6a) gave a major [M – H]<sup>-</sup> fragment ions at *m/z* 943, but the spectrum also contained many unrelated fragment ions (e.g., ions of *m/z* 957, 930, 921, and 905) that complicate the structural identification. These fragment ions may arise from the adjacent precursor ions admitted together with the desired DAT ions for CID, due to that the precursor ion selection window (1 Da) cannot sufficiently isolate the isobaric ions (the mass selection window and injection time govern the total ions admitted to the trap for CID and >1 Da mass selection window is often required to maintain the sensitivity). Thus, fragment ions unrelated to the targeted molecule were formed simultaneously and complicating the structure analysis. However, the MS<sup>3</sup> spectrum of *m/z* 943 (Figure 6b) contained only the fragment ions related to the DAT species, due to that the [M – H]<sup>-</sup> ions still retain the complete structure but have been further segregated, and fragment ions unrelated to the structure have been filtrated by another stage (MS<sup>3</sup>) isolation. In this context, the MS<sup>4</sup> spectrum of the ions of *m/z* 589 (989 → 943 → 589; Figure 6c), which were further “purified”, becomes even more specific, due to that only the fragment ions from DAT that consists of 23:0-FA substituent at C3 were subjected to further CID. Thus, the spectrum only contained ions of *m/z* 283, representing a 18:0-carboxylate anion, along with ions at *m/z* 323 and 305, representing the dehydrated trehalose anions. These results led to specifically define the 18:0/23:0-DAT structure. The spectrum (Figure 6b) also contained the

$m/z$  269/367 and 255/381 ion pairs, representing the 17:0/24:0-, 16:0/25:0-FA carboxylate anion pairs, together with ions of  $m/z$  687/561 and 673/575 ion pairs, arising from losses of 17:0/24:0-, 16:0/25:0-FA substituents, respectively. These results readily led to the assignment of 17:0/24:0- and 16:0/25:0-DAT isomeric structures.

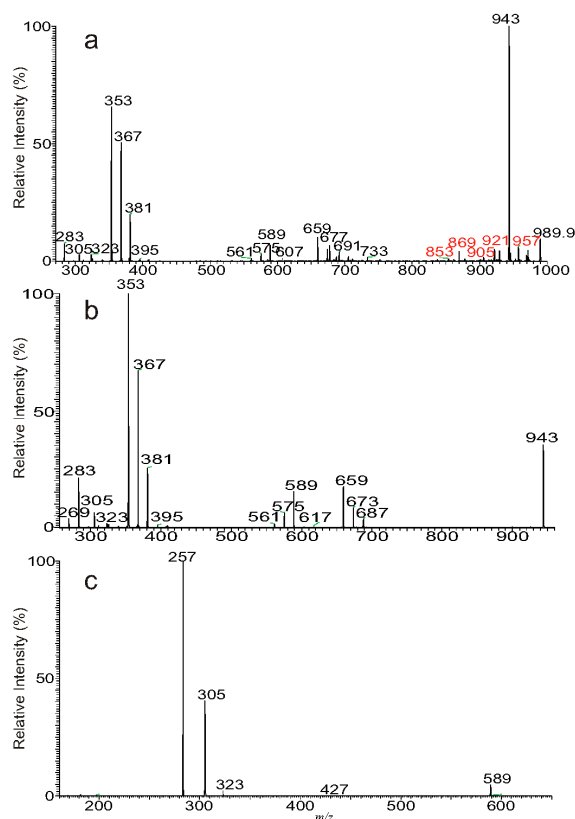


**Figure 6.** The negative-ion  $MS^2$  spectrum of the  $[M + HCO_2]^-$  ions of DAT at  $m/z$  989 (a), its  $MS^3$  spectrum of the ions of  $m/z$  943 ( $989 \rightarrow 943$ ) (b),  $MS^4$  spectrum of the ions of  $m/z$  589 ( $989 \rightarrow 943 \rightarrow 589$ ) (c). The ions of  $m/z$  989 are minor species and its  $MS^2$  spectrum contains several ions (shown in red in (a)) unrelated to the structure, but have been filtrated from higher stage  $MS^n$ , as shown in (b) ( $MS^3$ ) and (c) ( $MS^4$ ).

#### 4. Conclusions

Sequential precursor ion isolation applying multiple-stage mass spectrometry (LIT  $MS^n$ ) adds another dimension of separation in the analysis, providing a powerful tool for structural identification of various compounds. Thereby, many isomeric structures of the molecule can be unveiled in a very short period of time. By contrast, using the conventional chromatographic separation combined with a TSQ or QTOF instrument, the consecutive precursor ion isolation by MS is not achievable, and the species separation can only rely on column separation. Thus, complete separation of a complex lipid mixture with a wide range of molecular species and many isomeric structures is often difficult. Compound separation by chromatographic means also requires significantly more times [33], as compared to the LIT  $MS^n$  approach, by which the separation-CID-detection process can be completed within a very short period of time.

LIT  $MS^n$  permits ion isolation in the time sequence manner, and the separation of ions is flexible (i.e., the types of ions selected and the mass selection window of precursor ions). The selected ions become more specific, and the  $MS^n$  spectrum provides more structurally specific information as the  $MS^n$  stage advances, therefore, resulting in a confident and detailed structural identification. The structures of minute ion species that are often difficult to define by other analytical method can also be assigned (Table 1). However, the sensitivity declines as the higher order of  $MS^n$  stage proceeds.

Other drawback includes that a complete structural information is not necessary extractable by MS<sup>n</sup>. For example, the positions of the double bond and methyl side chain of the fatty acid substituents at C3 have not been defined in this study.

The LIT MS<sup>n</sup> approach as described here affords near complete structural characterization of a complex DAT lipid family, locating the fatty acyl groups on the trehalose backbone, and recognizing many isomeric structures. A LIT MS<sup>n</sup> approach combined with chemical reaction modification [9,34] for locating the functional groups including the methyl, hydroxyl, and the double bond on the fatty acid substituents are currently in progress in our laboratory.

**Author Contributions:** C.F. performs lipid separation; R.B.A. and G.E.P. grow cell and extract total lipids; L.L. and L.L. synthesize DAT standards. F.-F.H. performs mass spectrometry analysis and write the manuscript.

**Funding:** This research was funded by US Public Health Service Grants P41GM103422, P30DK020579, R01AI130454, R21AI128427, R21HL120760, and R21AI113074.

**Acknowledgments:** This research was supported by US Public Health Service Grants P41GM103422, P30DK020579, R01AI130454, R21AI128427, R21AI113074 and R21HL120760.

**Conflicts of Interest:** The authors declare no conflict of interest.

## Abbreviations

LIT, linear ion trap; MS<sup>n</sup>, multiple stage mass spectrometry; Glc, glucose; DAT, diacyltrehalose; FA, fatty acid; FA-ketene, fatty acyl ketene; CID, collision induced dissociation; ESI, electrospray ionization; HRMS, high-resolution mass spectrometry.

## References

1. Johnson, J.V.; Yost, R.A.; Kelley, P.E.; Bradford, D.C. Tandem-in-space and tandem-in-time mass spectrometry: triple quadrupoles and quadrupole ion traps. *Anal. Chem.* **1990**, *62*, 2162–2172. [[CrossRef](#)]
2. Markarov, A.; Cousijn, E.; Canterbury, J.; Denisov, E.; Thoeing, C.; Lange, O.; Kreutzman, A.; Ayzikov, K.; Damoc, E.; Tabiwang, A.; et al. Extension of Orbitrap capabilities to enable new applications. In Proceedings of the 65th Conference on Mass Spectrometry and Allied Topics, Indianapolis, IN, USA, 4 June 2017.
3. Vogel, C.; Marcotte, E.M. Insights into the regulation of protein abundance from proteomic and transcriptomic analyses. *Nat. Rev. Genet.* **2012**, *13*, 227–232. [[CrossRef](#)] [[PubMed](#)]
4. Perry, R.H.; Cooks, R.G.; Noll, R.J. Orbitrap mass spectrometry: Instrumentation, ion motion and applications. *Mass Spectrom. Rev.* **2008**, *27*, 661–699. [[CrossRef](#)] [[PubMed](#)]
5. Senyuva, H.Z.; Gökmen, V.; Sarikaya, E.A. Future perspectives in Orbitrap<sup>TM</sup>-high-resolution mass spectrometry in food analysis: A review. *Food Addit. Contam. A* **2015**, *32*, 1568–1606. [[CrossRef](#)] [[PubMed](#)]
6. Jabbour, R.E.; Snyder, A.P. Chap. 14—Mass spectrometry-based proteomics techniques for biological identification. In *Biological Identification*; Schaudies, R.P., Ed.; Woodhead Publishing: Sawston, UK, 2014; pp. 370–430.
7. Eliuk, S.; Makarov, A. Evolution of Orbitrap Mass Spectrometry Instrumentation. *Ann. Rev. Anal. Chem.* **2015**, *8*, 61–80. [[CrossRef](#)] [[PubMed](#)]
8. Rhoades, E.R.; Streeter, C.; Turk, J.; Hsu, F.-F. Characterization of Sulfolipids of *Mycobacterium tuberculosis* H37Rv by Multiple-Stage Linear Ion-Trap High-Resolution Mass Spectrometry with Electrospray Ionization Reveals That the Family of Sulfolipid II Predominates. *Biochemistry* **2011**, *50*, 9135–9147. [[CrossRef](#)] [[PubMed](#)]
9. Hsu, F.-F. Characterization of Hydroxyphthioceranoic and Phthioceranoic Acids by Charge-Switch Derivatization and CID Tandem Mass Spectrometry. *J. Am. Soc. Mass Spectrom.* **2016**, *27*, 622–632. [[CrossRef](#)]
10. Hsu, F.F.; Turk, J.; Owens, R.M.; Rhoades, E.R.; Russell, D.G. Structural Characterization of Phosphatidyl-myo-Inositol Mannosides from *Mycobacterium bovis* Bacillus Calmette Guerin by Multiple-Stage Quadrupole Ion-Trap Mass Spectrometry with Electrospray Ionization. II. Monoacyl- and Diacyl-PIMs. *J. Am. Soc. Mass Spectrom.* **2007**, *18*, 479–492. [[CrossRef](#)]
11. Hsu, F.F.; Turk, J.; Owens, R.M.; Rhoades, E.R.; Russell, D.G. Structural characterization of phosphatidyl-myo-inositol mannosides from *Mycobacterium bovis* Bacillus Calmette Guerin by multiple-stage quadrupole ion-trap mass spectrometry with electrospray ionization. I. PIMs and lyso-PIMs. *J. Am. Soc. Mass Spectrom.* **2007**, *18*, 466–478. [[CrossRef](#)]

12. Flentie, K.N.; Stallings, C.L.; Turk, J.; Minnaard, A.J.; Hsu, F.-F. Characterization of phthiocerol and phthiodiolone dimycocerosate esters of *M. tuberculosis* by multiple-stage linear ion-trap MS. *J. Lipid Res.* **2016**, *57*, 142–155. [[CrossRef](#)]
13. Hoppe, H.C.; de Wet, B.J.; Cywes, C.; Daffe, M.; Ehlers, M.R. Identification of phosphatidylinositol mannoside as a mycobacterial adhesin mediating both direct and opsonic binding to nonphagocytic mammalian cells. *Infect. Immun.* **1997**, *65*, 3896–3905. [[PubMed](#)]
14. Howard, N.C.; Marin, N.D.; Ahmed, M.; Rosa, B.A.; Martin, J.; Bambouskova, M.; Sergushichev, A.; Loginicheva, E.; Kurepina, N.; Rangel-Moreno, J.; et al. Mycobacterium tuberculosis carrying a rifampicin drug resistance mutation reprograms macrophage metabolism through cell wall lipid changes. *Nat. Microbiol.* **2018**, *3*, 1099–1108. [[CrossRef](#)] [[PubMed](#)]
15. Daffé, M.; Lacave, C.; Lanéelle, M.-A.; Gillois, M.; Lanéelle, G. Polyphthienoyl trehalose, glycolipids specific for virulent strains of the tubercle bacillus. *Eur. J. Biochem.* **1988**, *172*, 579–584. [[CrossRef](#)] [[PubMed](#)]
16. Minnikin, D.E.; Dobson, G.; Sesardic, D.; Ridell, M. Mycolipenates and Mycolipanolates of Trehalose from *Mycobacterium tuberculosis*. *J. Gen. Microbiol.* **1985**, *131*, 1369–1374. [[CrossRef](#)] [[PubMed](#)]
17. Munoz, M.; Laneelle, M.A.; Luquin, M.; Torrelles, J.; Julian, E.; Ausina, V.; Daffe, M. Occurrence of an antigenic triacyl trehalose in clinical isolates and reference strains of *Mycobacterium tuberculosis*. *FEMS Microbiol. Lett.* **1997**, *157*, 251–259. [[CrossRef](#)]
18. Lemassu, A.; Laneelle, M.A.; Daffe, M. Revised structure of a trehalose-containing immunoreactive glycolipid of *Mycobacterium tuberculosis*. *FEMS Microbiol. Lett.* **1991**, *62*, 171–175. [[CrossRef](#)] [[PubMed](#)]
19. Ariza, M.A.; Martín-Luengo, F.; Valero-Guillén, P.L. A family of diacyltrehaloses isolated from *Mycobacterium fortuitum*. *Microbiology* **1994**, *140*, 1989–1994. [[CrossRef](#)] [[PubMed](#)]
20. Ariza, M.A.; Valero-Guillen, P.L. Delineation of molecular species of a family of diacyltrehaloses from *Mycobacterium fortuitum* by mass spectrometry. *FEMS Microbiol. Lett.* **1994**, *119*, 279–282. [[CrossRef](#)]
21. Besra, G.S.; Bolton, R.C.; McNeil, M.R.; Ridell, M.; Simpson, K.E.; Glushka, J.; Van Halbeek, H.; Brennan, P.J.; Minnikin, D.E. Structural elucidation of a novel family of acyltrehaloses from *Mycobacterium tuberculosis*. *Biochemistry* **1992**, *31*, 9832–9837. [[CrossRef](#)]
22. Gautier, N.; Marín, L.M.L.; Lanéelle, M.A.; Daffé, M. Structure of mycoside F, a family of trehalose-containing glycolipids of *Mycobacterium fortuitum*. *FEMS Microbiol. Lett.* **1992**, *77*, 81–87.
23. Lee, K.-S.; Dubey, V.S.; Kolattukudy, P.E.; Song, C.-H.; Shin, A.R.; Jung, S.-B.; Yang, C.-S.; Kim, S.-Y.; Jo, E.-K.; Park, J.-K.; et al. Diacyltrehalose of *Mycobacterium tuberculosis* inhibits lipopolysaccharide- and mycobacteria-induced proinflammatory cytokine production in human monocytic cells. *FEMS Microbiol. Lett.* **2007**, *267*, 121–128. [[CrossRef](#)] [[PubMed](#)]
24. Saavedra, R.; Segura, E.; Leyva, R.; Esparza, L.A.; López-Marín, L.M. Mycobacterial Di-O-Acyl-Trehalose Inhibits Mitogen- and Antigen-Induced Proliferation of Murine T Cells In Vitro. *Clin. Diagn. Lab. Immunol.* **2001**, *8*, 1081–1088. [[CrossRef](#)]
25. Bailo, R.; Bhatt, A.; Ainsa, J.A. Lipid transport in *Mycobacterium tuberculosis* and its implications in virulence and drug development. *Biochem. Pharmacol.* **2015**, *96*, 159–167. [[CrossRef](#)] [[PubMed](#)]
26. Papa, F.; Cruaud, P.; David, H.L. Antigenicity and specificity of selected glycolipid fractions from *Mycobacterium tuberculosis*. *Res. Microbiol.* **1989**, *140*, 569–578. [[CrossRef](#)]
27. Hamid, M.E.; Fraser, J.L.; Wallace, P.A.; Besra, G.; Goodfellow, M.; Minnikin, D.E. Antigenic glycolipids of *Mycobacterium fortuitum* based on trehalose acylated with 2-methyloctadec-2-enoic acid. *Lett. Appl. Microbiol. Rev.* **1993**, *16*, 132–135. [[CrossRef](#)]
28. Ridell, M.; Wallerström, G.; Minnikin, D.E.; Bolton, R.C.; Magnusson, M. A comparative serological study of antigenic glycolipids from *Mycobacterium tuberculosis*. *Tubercle Lung Dis.* **1992**, *73*, 71–75. [[CrossRef](#)]
29. Tórtola, M.T.; Lanéelle, M.A.; Martín-Casabona, N. Comparison of two 2,3-diacyl trehalose antigens from *Mycobacterium tuberculosis* and *Mycobacterium fortuitum* for serology in tuberculosis patients. *Clin. Diagn. Lab. Immunol.* **1996**, *3*, 563–566.
30. Prabhakar, S.; Vivès, T.; Ferrières, V.; Benvegnu, T.; Legentil, L.; Lemiègre, L. A fully enzymatic esterification/transesterification sequence for the preparation of symmetrical and unsymmetrical trehalose diacyl conjugates. *Green Chem.* **2017**, *19*, 987–995. [[CrossRef](#)]
31. Botté, C.Y.; Deligny, M.; Roccia, A.; Bonneau, A.-L.; Saïdani, N.; Hardré, H.; Aci, S.; Yamaryo-Botté, Y.; Jouhet, J.; Dubots, E.; et al. Chemical inhibitors of monogalactosyldiacylglycerol synthases in *Arabidopsis thaliana*. *Nat. Chem. Biol.* **2011**, *7*, 834–842. [[CrossRef](#)]

32. Olsen, J.V.; Macek, B.; Lange, O.; Makarov, A.; Horning, S.; Mann, M. Higher-energy C-trap dissociation for peptide modification analysis. *Nat. Meth.* **2007**, *4*, 709–712. [[CrossRef](#)]
33. Hsu, F.F. Mass spectrometry-based shotgun lipidomics—A critical review from the technical point of view. *Anal. Bioanal. Chem.* **2018**, *410*, 6387–6409. [[CrossRef](#)] [[PubMed](#)]
34. Frankfater, C.; Jiang, X.; Hsu, F.F. Characterization of Long-Chain Fatty Acid as N-(4-Aminomethylphenyl) Pyridinium Derivative by MALDI LIFT-TOF/TOF Mass Spectrometry. *J. Am. Soc. Mass Spectrom.* **2018**, *29*, 1688–1699. [[CrossRef](#)] [[PubMed](#)]



© 2019 by the authors. Licensee MDPI, Basel, Switzerland. This article is an open access article distributed under the terms and conditions of the Creative Commons Attribution (CC BY) license (<http://creativecommons.org/licenses/by/4.0/>).